Journal of Power Sources 203 (2012) 26–33

Contents lists available at SciVerse ScienceDirect

Journal of Power Sources

journal homepage: www.elsevier.com/locate/jpowsour

Nanostructured design of electrocatalyst support materials for high-performance PEM fuel cell application

Ratna Balgis[a], Gopinathan M. Anilkumar[b], Sumihito Sago[b], Takashi Ogi[a,*], Kikuo Okuyama[a]

[a] Department of Chemical Engineering, Graduate School of Engineering, Hiroshima University, 1-4-1 Kagamiyama, Higashi-Hiroshima 739-8527, Japan
[b] Research and Development Centre, Noritake, Co., Ltd., 300 Higashiyama-Miyoshi, Aichi 470-0293, Japan

ARTICLE INFO

Article history:
Received 23 September 2011
Received in revised form
21 November 2011
Accepted 21 November 2011
Available online 17 December 2011

Keywords:
Electrocatalyst
Proton exchange membrane fuel cell (PEMFC)
Catalyst support
Particle morphology
Mass activity

ABSTRACT

Carbon-supported platinum (Pt/C) catalysts with controlled morphologies, namely, "*dense-erythrocyte-like* (DEL)" and "*hollow-porous-microsphere* (HPM)" have been synthesized by spray-drying followed by impregnation of 10 wt.% of Pt nanoparticles. Addition of polystyrene latex (PSL) template particles plays a crucial role to determine the carbon morphology, which was confirmed by SEM and TEM images. The preparation of modified catalyst support was completed in only several seconds for DEL and less than 1 h for HPM, which is contrary to currently available methods that require time up to several days to complete the modified catalyst support synthesize. Pt nanoparticles are agglomeration-free, and well-dispersed on the surface of the carbon particles with the size around 4 nm. The electrocatalytic activity of the modified Pt/C catalyst particles was comparable to that of a commercially available Pt/C catalyst (TKK). The specific activity of the Pt/C_{HPM} catalyst was 2 times higher than that of Pt/C_{DEL} catalyst, and was up to 2.5 times than that of the commercial one. The mass activity of Pt/C_{HPM} was 239.57 mA mg^{-1} Pt and also shows a great enhancement, about 1.55 times higher than the commercial.

1. Introduction

Catalyst design is one of the most challenging subjects in electrochemistry. Successful design of catalysts allows us to produce high-performance proton exchange membrane fuel cells (PEMFCs), which are very promising as future energy sources. Platinum (Pt) is widely used as an excellent catalyst for electrochemical reaction in PEMFCs. However, its low-level abundance in nature creates a great barrier for the commercialization of PEMFCs [1,2]. Much effort has been made, not only to reduce Pt content but also to enhance catalytic activity [3,4]. Alloying Pt with other less expensive metals, such as Pd, Ni, Co, V, and Cr, is an effective approach to reduce Pt amount [5–7]. However, stability and durability problems of such Pt-alloys remain unsolved [8,9].

Another strategy to reduce Pt amount and increase the durability is enhancing the interaction between the catalyst and the support material [10–12]. Catalyst support strongly influences the particle size and dispersion of catalyst metal [13–15]. Furthermore, catalytic performance can be finely tuned by varying the composition and/or structure of the catalyst support. A structure with high surface area is highly desirable for catalyst support. Carbon black has been a standard catalyst support for PEMFCs applications [16–18]. However, carbon black contains micropores which can trap Pt particles, resulting in low-performance fuel cells [19]. The addition of perfluorosulfonate ionomer (PSFI) and polutetrafluoroethylene (PTFE) may influence the catalytic activity [20–22]. Carbon black with morphological modification provides more promising solution for this restriction [23,24]. The structural engineering of carbon nanoparticles into carbon microspheres would allow good dispersion of Pt nanoparticles and rapid transport of reactant and product from the active catalytic sites to the bulk of the fluid [25–28]. Although the morphological control of Pt/C catalyst has been reported, the electrochemical activity of these catalysts is still unsatisfactory. In addition, complex and time-consuming preparation process creates a great barrier for its functionalization, especially for industrial application. For example, Pylypenko et al. [11] prepared porous Pt/C catalyst employing silica as a template. The pores structure of carbon supporter prevented the agglomeration of Pt nanoparticle. However, the procedures were very complicated and time consuming, and also the catalyst performance was lower than expected due to lower number of transferred electrons per redox event and/or additional diffusion limitations in the pores of the template material. Kim and Yu [14] synthesized erythrocyte-like hollow carbon capsules with high catalyst performance; however, the procedures were very complicated.

The present study reports a facile route to design Pt/C catalysts using carbon microspheres with controlled morphology at

* Corresponding author. Tel.: +81 82 424 7850; fax: +81 82 424 5494.
E-mail address: ogit@hiroshima-u.ac.jp (T. Ogi).

0378-7753/$ – see front matter © 2011 Elsevier B.V. All rights reserved.
doi:10.1016/j.jpowsour.2011.11.064

a high production rate. Microspherical carbon was prepared by spray-drying, followed by impregnation of 10 wt.% of Pt nanoparticles. Morphological control of carbon microspheres (dense and hollow-porous) was done by simply adding the template particles to the precursor prior to spray-drying [29]. This is the first report on the investigation of catalyst performance influenced by nanostructure engineering of catalyst support employing spray-drying method. The results of this method were then examined for catalyst application in PEMFCs.

2. Experimental

2.1. Preparation of modified catalyst support

An aqueous slurry consisting of 0.224 wt.% carbon nanoparticles (40 nm, Mikuni Color Co., Ltd., Japan) was spray dried at 210 °C using a commercial mini spray dryer (BÜCHI B-290) to obtain dense-erythrocyte-like particles, called DEL carbon. In another experiment, homemade polystyrene latex (PSL, 300 nm) beads were added to the carbon slurry to control the morphology of the prepared particles. The ratio of PSL:carbon was 1.3:1 and sprayed at the same condition as DEL carbon. The composite was then reheated at 600 °C for 5 min to decompose the PSL and obtained hollow-porous-microsphere particles, called HPM carbon. A detailed explanation of the spray-drying process can be found in our previous work [29].

2.2. Catalyst deposition on modified carbon support

To facilitate the Pt impregnation process, 100 g of aqueous polymer solution containing 10 mg of polyvinyl alcohol (PVA, M_w = 500, Cica-reagent, Kanto Chemical Co. Inc., Japan) was used. The modified-carbon supporter (DEL or HPM) and 10 wt.% of chloroplatinic acid dispersion (Noritake Co., Ltd., Japan) ($H_2PtCl_6{\cdot}6H_2O$) were added to the polymer solution and stirred for 1 h. The mass ratio of PVA, carbon microspheres, and chloroplatinic acid was kept constant at 1:10:1. Chloroplatinic acid was then reduced using 20 mL of 1 M sodium borohydride ($NaBH_4$) solution under vigorous stirring for 5 h. The solution was aged overnight, washed, dried at 80 °C for 30 min, and reheated at 120 °C for 2 h in a vacuum furnace to clean the surface of the Pt catalyst.

2.3. Pt/C catalyst material characterization

The morphology of the particles was observed using a field emission scanning electron microscope (FE-SEM, Hitachi, S-5000, 20 kV) and a transmission electron microscope (TEM, JEOL-JEM-2010, 200 kV). The surface area was determined quantitatively using N_2 adsorption–desorption by the Brunauer, Emmet, and Teller (BET) method. Pt content in the catalyst was measured using an inductively coupled plasma (ICP) mass spectrometer (SII, SPS-3000). The crystal structure was characterized by X-ray diffraction (XRD, Rigaku, RINT2000).

2.4. Electrochemical characterization

Electrochemical characterization of prepared catalyst was performed using cyclic voltammetry (CV) and rotating disc electrode (RDE) (Hokuto-denko, HR-301). Catalyst ink was prepared by dispersing 18.5 mg catalyst in the mixture of 6 mL isopropanol (Cica-reagent, Kanto Chemical Co. Inc., Japan) and 19 mL ultrapure water. A 100 μL of Nafion® dispersion solution (5 wt.%, Wako Pure Chemical Industries, Ltd., Japan) was added, then placed the mixture of catalyst ink in an ice bath and sonicated for 30 min [30]. Ten microliters of catalyst ink was transferred onto the polished glassy carbon disk (Ø = 5 mm, geometric area = 0.196 cm^2) and dried to form a thin catalyst layer. The Pt loading on the glassy carbon was 7.4, 5.5, and 17.3 μg Pt cm^{-2} for Pt/C_{HPM}, Pt/C_{DEL}, and commercial Pt/C catalysts, respectively.

The measurement setup was a typical three-electrode system, consist of a working electrode (Pt/C on glassy carbon), a Pt wire as counter electrode, and a reversible H_2 electrode (RHE) as reference electrode. All measurements were performed at room temperature (~25 °C) using a fresh electrolyte solution (0.1 M $HClO_4$, Cica-reagent, Kanto Chemical Co. Inc., Japan). Nitrogen was flowed at 200 mL min^{-1} through the electrolyte solution for 10 min during each CV measurement to de-oxygenate the environment. The CV measurements were scanned between 0 and 1.2 V vs. RHE with a sweep rate of 50 mV s^{-1}. The saturation gas was switched to O_2 for RDE measurement, and the electrolyte was saturated for the same condition as CV measurement. Rotation rate was controlled at 400, 900, 1600, 2500, and 3600 rpm to collect data for Koutecký–Levich plots. Measurements were carried out at 10 mV s^{-1} sweep rates in a typical polarization program of 0.2 V → 1.2 V. The background current was measured by running the oxygen-reduction-reaction (ORR) sweep profile without any rotation in N_2-purged 0.1 M $HClO_4$ before the ORR measurement to eliminate any contributions of capacitive current.

3. Results and discussions

3.1. Morphology characteristic of the Pt/C catalyst

Morphological control of carbon microspheres can be understood as a consequence of droplet shape transformation during spray-drying. It is well known that the droplet shape in a dynamic fluid can be characterized by Bond number, defined as,

$$B = \frac{\Delta\rho a d^2}{\gamma}, \tag{1}$$

where B is Bond number, $\Delta\rho$ is the difference in the densities of the droplet and the surrounding fluid, a is the acceleration of the droplet, d is the largest radius of the circular horizontal cross section of the droplet, and γ is the interfacial tension. The droplet is spherical as the value of $B \to 0$, and flattens as the value of B increases [31]. In the present study, the difference in the densities of the droplets and surrounding medium can be described as

$$\Delta\rho = \rho_d - \rho_{air}, \tag{2}$$

where ρ_d is the density of the droplet and ρ_{air} is the density of air [32]. Since each precursor contains more than one object, the density of the droplets is expressed as a summation of each density times mass fraction, which can be described as follows:

$$\rho_d = \sum_{i=1}^{N} \phi_i \rho_i, \tag{3}$$

where ρ_i is the density of each object, ϕ_i is the mass fraction of each object, and N is the number of objects. The mass fraction, ϕ_i, follows the conservation law, which is described as follows:

$$\sum_{i=1}^{N} \phi_i = 1. \tag{4}$$

Eq. (1) shows an opportunity to control the particle morphology, from spherical to doughnut-type, by adjusting the value of $(\Delta\rho/\gamma)$, as illustrated in Fig. 1. The addition of PSL may decrease density of the droplet, therefore spherical morphology was obtained. Furthermore, particles assemblies in droplets also determine the final morphology of spray-dried particles. In a mixture of two particles with significant, different sizes (i.e. 40 nm carbon particles

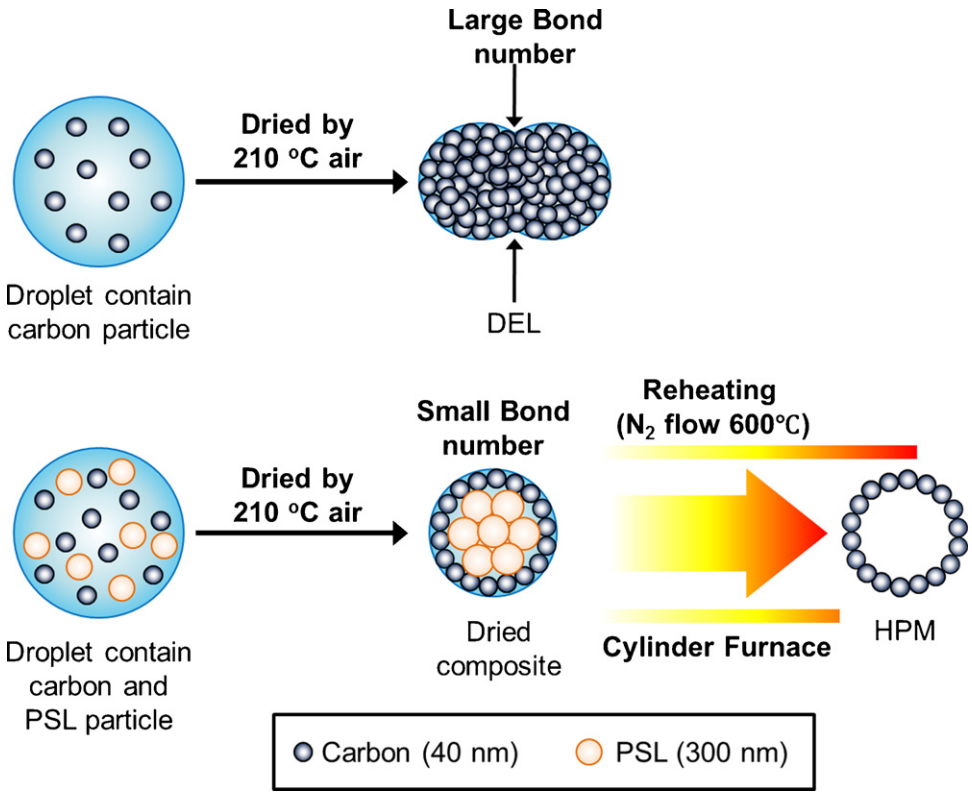

Fig. 1. Schematic diagram of the formation of dense and hollow-porous carbon particles by spray-dying.

and 300 nm PSL), carbon particles were carried through the interstices of the PSL during the drying process. The particles were ultimately deposited and aggregated, on the surface from which the last traces of water evaporated [31]. The composite was leaving hollow morphology when the PSL particles were removed by reheating treatment.

Fig. 2 shows a successful application of the spray-drying method to control the morphology of the carbon microspheres. The morphology of carbon microspheres was dense with a double-concave shape forming an erythrocyte-like structure labeled as "*dense-erythrocyte-like* (DEL)", which is shown in Fig. 2(a). The addition of PSL particles significantly changed the morphology to hollow-porous-microsphere structures, labeled as "*hollow-porous-microsphere* (HPM)", which is shown in Fig. 2(b). The optimum mass ratio of PSL to carbon black to obtain the hollow-porous structure was 1.3. Reheating treatment at 600 °C for 5 min under a nitrogen atmosphere was necessary to remove the PSL particles and form a hollow-porous structure. Both of the prepared carbon microspheres had a relatively narrow size distribution with average particle sizes of 3.6 and 3.97 μm for DEL and HPM carbon, respectively. The pore size of HPM carbon can be engineered to uniform, bimodal, and even to polydisperse size distribution by changing and mixing the PSL size.

The specific surface area was also calculated using the Brunauer–Emmet–Teller (BET) equation based on the measurement of nitrogen adsorption/desorption. The adsorption–desorption isotherm curves of DEL and HPM carbon are shown in Fig. 3(a) and (b), respectively. Both of the isotherm curves characterized the initial rapid rise of gas volume adsorbed with increasing relative pressure turning to a slow increase. The inflection point ($0.05 \leq P/P_0 \leq 0.3$) corresponded to both the completion of the monolayer coverage and the filling of the pores by capillary condensation. The rest of the curve corresponded to a normal multi-layer formation. These represent type II isotherm curves, which are usually encountered for nonporous particles or particles with pore diameters larger than micropores. For all the isotherm curves (Fig. 3a and b), adsorption and desorption curves overlapped completely in the low relative pressure range, while the hysteresis loop existed in the high relative pressure ($P/P_0 \geq 0.8$) for dense carbon, which might have been due to the presence of an ink-bottle type of pores [33]. This pore type confirmed that even though the dense particles contained some pores due to the voids between carbon particles, the pores were dead ends and finally formed a dense morphology. The adsorbed nitrogen volume of the hollow-porous particles was slightly greater than that of the dense particles at higher relative pressure (P/P_0) indicating a greater pore size distribution for those samples corresponding to the presence of voids between the carbon particle and the pores formed by PSL decomposition. The specific surface area (S_{BET}) of the DEL and HPM carbon microspheres was about 73.37 and 91.45 $m^2\,g^{-1}$, respectively. These results led to a hypothesis that the value of $\left(\Delta\rho/\gamma\right)$ for the precursor contained PSL particles was smaller than for another precursor; therefore, a hollow porous structure was formed.

Functionalization of carbon microspheres as a catalyst support was done via Pt impregnation (~10 wt.%) on the surface of the carbon microspheres mediated by PVA. PVA very effectively inhibits aggregation and controls the size of noble-metal nanoparticles [34,35]. SEM and TEM images confirmed the presence of Pt nanoparticles on the surface of DEL (Fig. 4a–c) and HPM (Fig. 4d–f) carbon microspheres. A TEM image of Fig. 4(e) also reveals that produced particle has hollow structure. It is interesting to see that on Pt/C_{HPM}, the Pt nanoparticles were deposited both on outer and inner surfaces, even in the cavities (Fig. 5). In both types, Pt nanoparticles were agglomeration-free and well dispersed as confirmed by elemental mapping shown in Fig. 6. The mean diameters of Pt nanoparticles were 3.94 nm (on Pt/C_{DEL}) and 3.88 nm (on Pt/C_{HPM}). Qualitatively, the amount of Pt nanoparticles contained

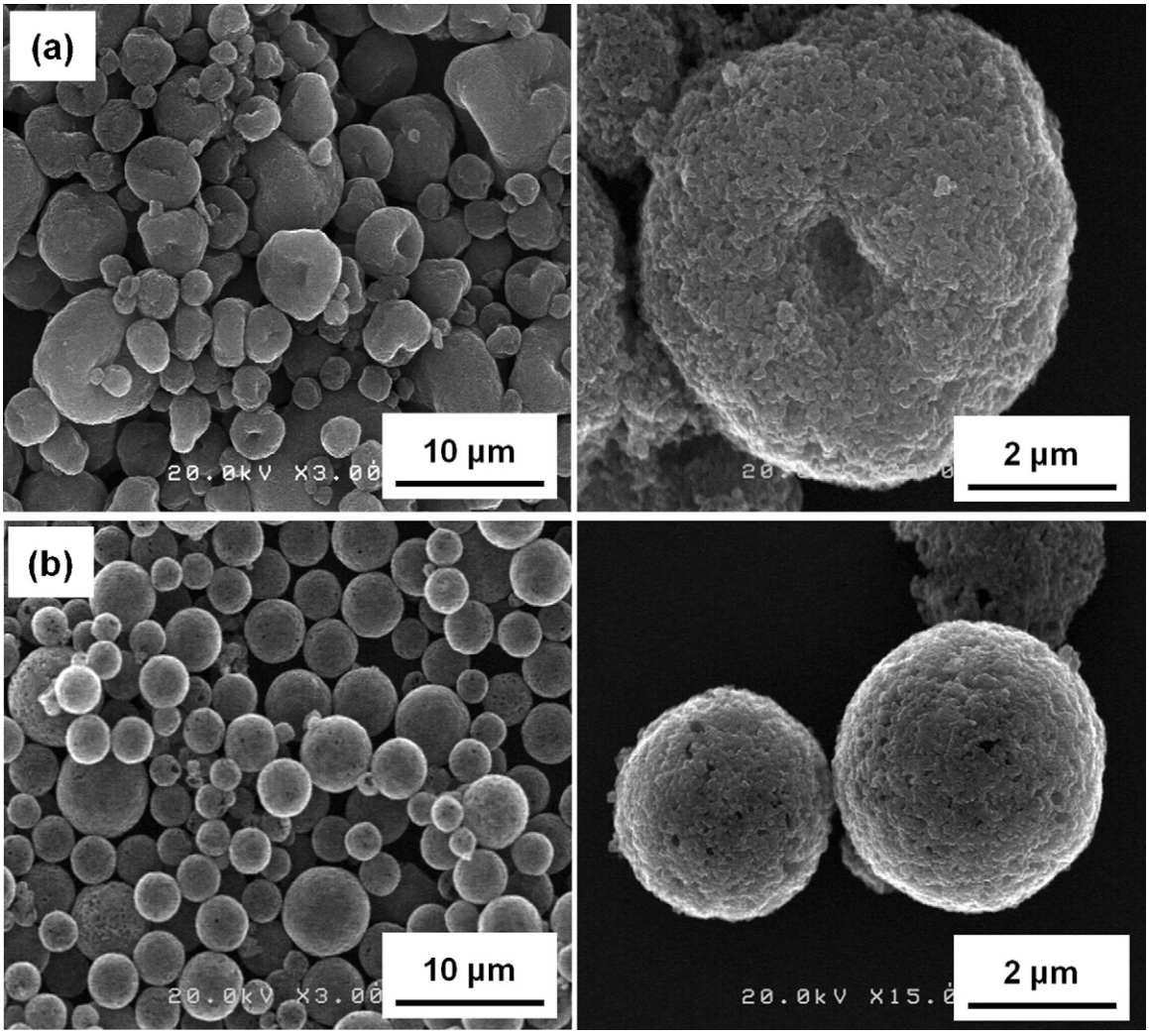

Fig. 2. FE-SEM images of (a) DEL and (b) HPM carbon.

in the hollow-porous carbon was greater than the amount of Pt nanoparticles contained in the dense carbon as confirmed by ICP measurement. It might be due to the finding that surface area of hollow-porous carbon was higher than that of dense carbon. The actual Pt loading on the carbon microspheres was 9.9 and 7.3 wt.% for Pt/C_{HPM} and Pt/C_{DEL}, which deviated slightly from the prepared precursor.

Fig. 7 shows the XRD patterns of the prepared Pt/C catalyst sample. The XRD pattern of both catalysts showed broad peaks around 25° (2θ) that corresponded to the diffraction of carbon black. The

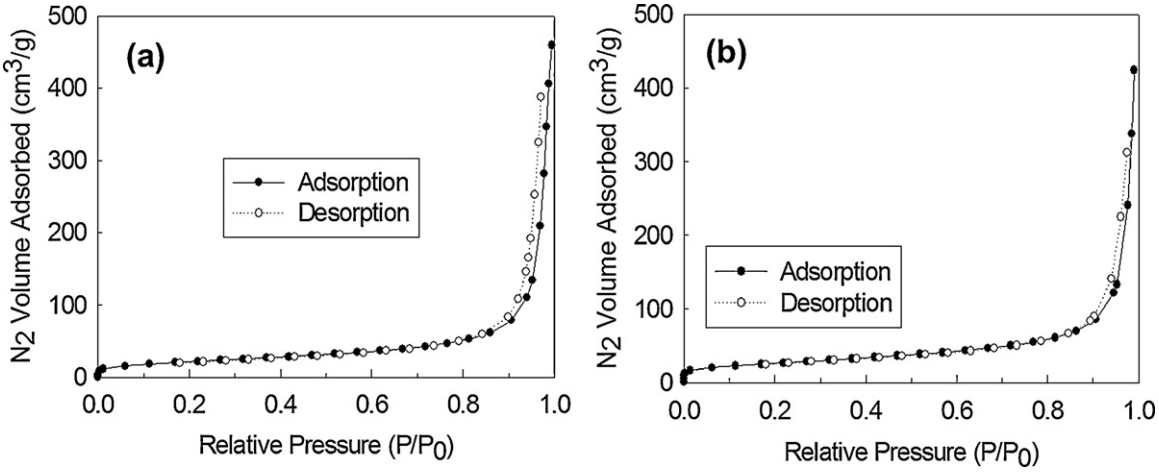

Fig. 3. Nitrogen adsorption isotherm curves of (a) DEL and (b) HPM carbon.

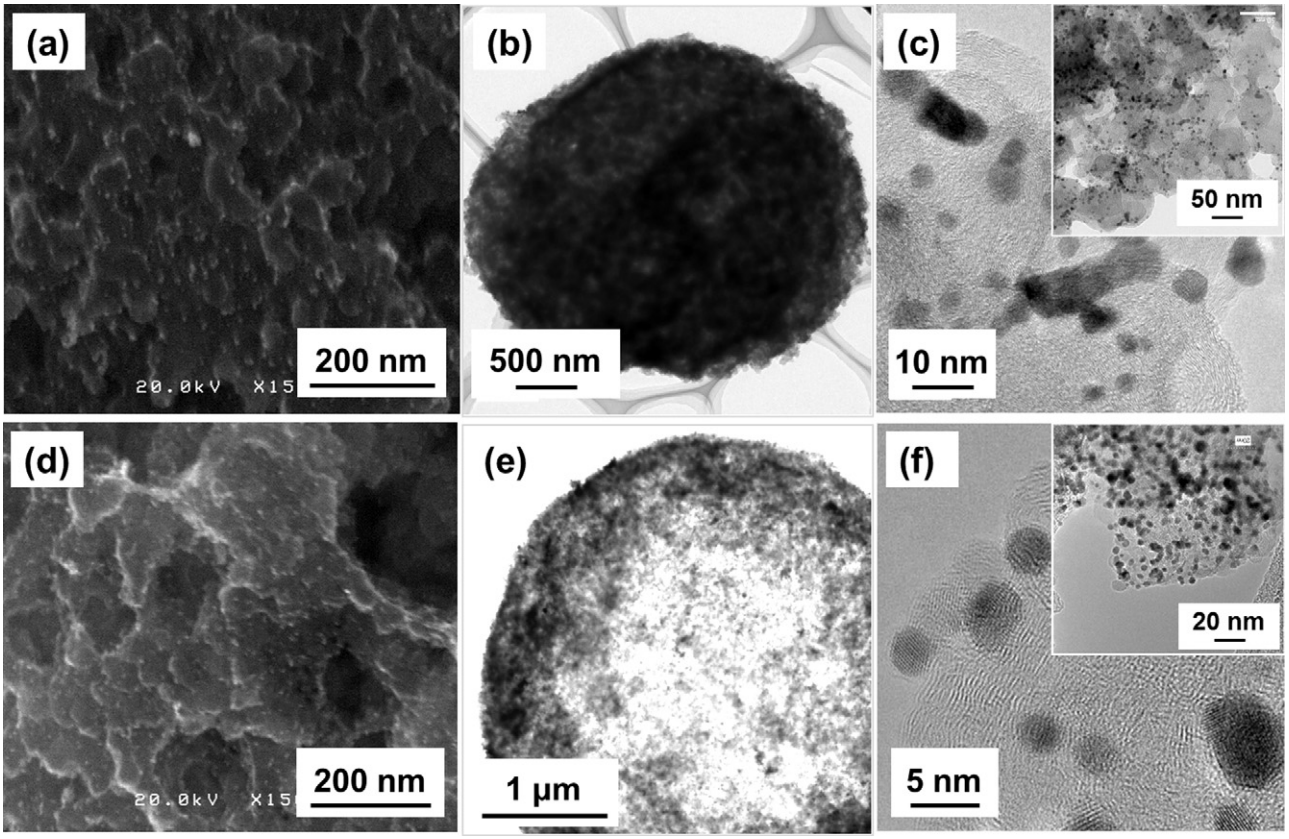

Fig. 4. High-resolution FE-SEM and TEM images of (a–c) Pt/C_{DEL} and (d–f) Pt/C_{HPM} catalysts.

diffraction peaks of Pt were observed at 39°, 46° and 68° (2θ) corresponding to the crystalline planes of (1 1 1), (2 0 0) and (2 2 0), respectively (JCPDS Card No. 4-0802), with a face-centered cubic (fcc) crystal structure. The crystallite sizes of Pt nanoparticles, calculated by Scherrer equation, were 3.86 and 3.95 nm for Pt/C_{DEL} and Pt/C_{HPM}, respectively. The XRD patterns were refined using a Gaussian approach prior to calculation, as shown in the insets of Fig. 7. The crystallite sizes of the Pt were almost equal to the diameters of the Pt nanoparticles calculated from TEM images. The diffraction peaks of Pt proved that the reduction of chloroplatinic acid by sodium borohydride had been achieved. The XRD patterns did not differ significantly, indicating that the morphology of the carbon microspheres did not contribute greatly to the crystal growth of Pt nanoparticles.

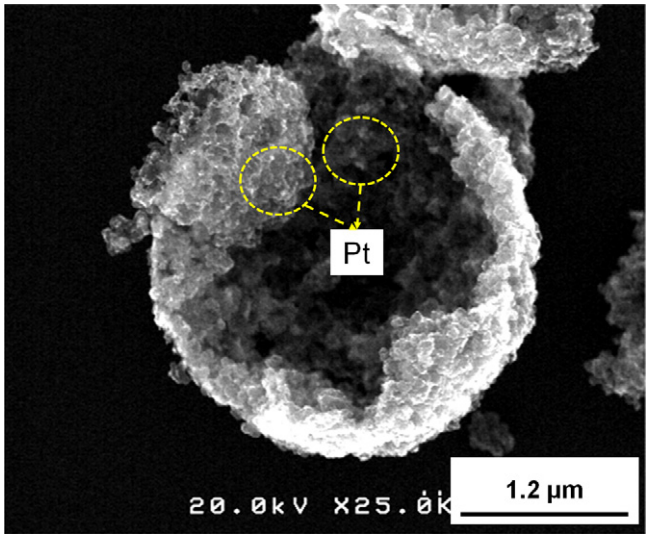

Fig. 5. FE-SEM images of broken Pt/C_{HPM} catalyst showing Pt deposition both on outer and inner surfaces of the catalyst.

3.2. Electrochemical characterization

The electrochemical characteristics of the prepared Pt/C catalysts are represented by CV and ORR polarization curves. In order to examine the figure of merit of prepared catalysts, the electrochemical characteristics of commercial Pt/C catalyst (46.1 wt.%) purchased from Tanaka Kikinzoku Kogyo Co., Ltd. (TKK) was also measured. The electrical properties of commercial carbon-supported Pt nanoparticles (Pt/C) were measured under the same conditions as the Pt/C_{DEL} and Pt/C_{HPM} catalysts.

Fig. 8 shows the adsorption/desorption characteristics of the Pt/C_{DEL}, Pt/C_{HPM}, and commercial Pt/C catalysts. As for prepared Pt/C catalyst, a weak adsorption of hydrogen ion peak in the potential range from 0.4 to 0.13 V and a strong adsorption peak located between 0.13 and 0.02 V were observed during the negative-going potential scan, and were assigned to weakly and strongly bonded hydrogen atoms, respectively. H_2 generation was obtained at the lower potential. The electrochemical surface area (ECSA) of the Pt in the working electrode is calculated using the hydrogen adsorption charge ($Q_{H\text{-adsorption}}$) limited by minimum potential which is selected just above the potential of H_2 generation onwards [1,30,36,37] (between 0.4 and ~0.05 V) as shown in Fig. S1 (Supporting Information). Corresponding desorption peaks were observed during the reserve potential scan. The ECSA were calculated at 54.18, 40.98, and 80.47 $m^2\ g^{-1}$ Pt for Pt/C_{HPM}, Pt/C_{DEL}, and commercial Pt/C, respectively. The ECSA of Pt/C_{DEL} catalyst was lower than Pt/C_{HPM} catalyst probably due to the low surface area, and might be there a possibility for Pt nanoparticles to

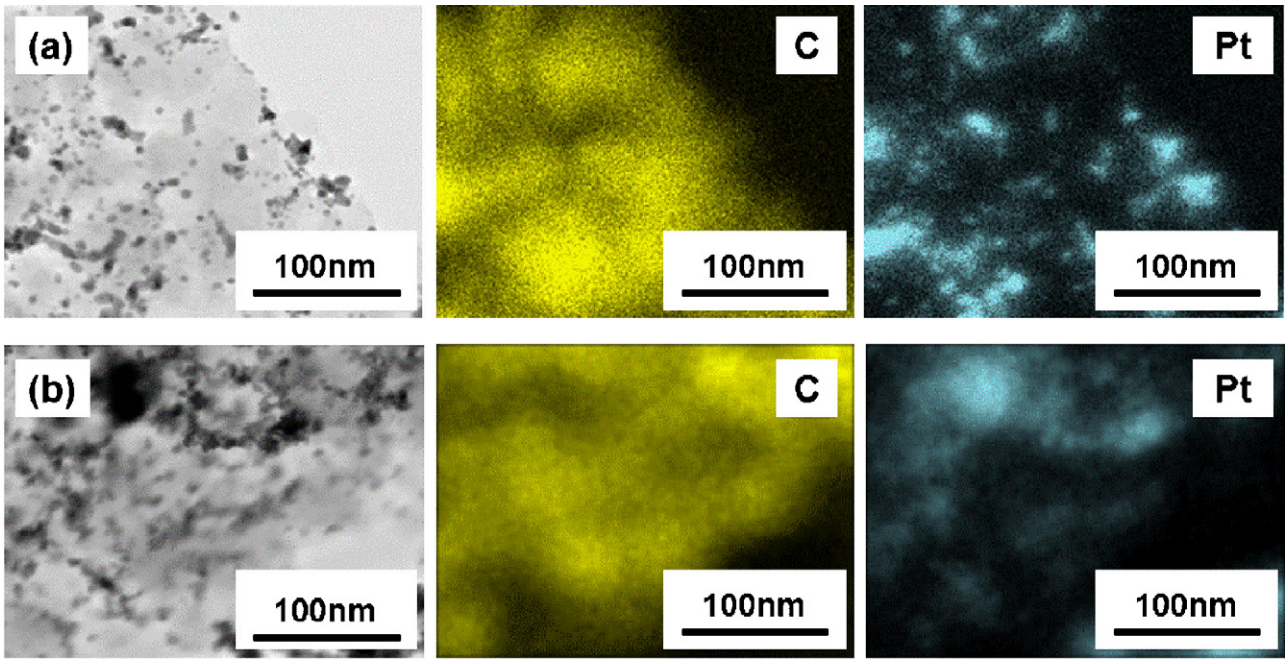

Fig. 6. Chemical mapping of (a) Pt/C_{DEL} and (b) Pt/C_{HPM} catalysts.

agglomerate during the catalytic activity measurement that inhibits the mobility of electron as mentioned in previous studies [38,39]. On the other hand, the ECSA of Pt/C_{HPM} catalyst was higher due to the high surface area and interconnected bimodal pore system of the hollow-porous structure that allows the diffusion and escape of reactant and product from the catalyst surface, thus shortening their stay time, as illustrated in Fig. 9. In PEMFCs, the catalyst will be embedded in a matrix of ionomer to operate the catalyst effectively. The pore size of Pt/C_{HPM} catalyst can be adjusted easily as mentioned in Section 3.1, we believe that this method allows the ionomer to pass through the Pt/C_{HPM} porous shell and finally exists in an inner wall of Pt/C_{HPM} catalyst without blocking the catalyst pores. Thus, it will not inhibit the fuel gas flow. Adjustment of pore size to the bimodal size distribution (mesopores and macropores) will optimize the transport phenomena in Pt/C_{HPM} catalyst. Mesopores allow the fuel gas flow effectively and keep the high surface area, whereas the macropores allow the ionomer to pass into Pt/C_{HPM} catalyst.

Oxygen reduction polarization curves of Pt/C_{DEL}, Pt/C_{HPM}, and commercial Pt/C recorded at different rotation speeds are presented in Fig. 10(a)–(c). The diffusion-limiting current density expected for materials that support direct $4e^-$ transfers, i.e., Pt-based electrodes, usually ranges between −5 and −6 mA cm^{-2} [27]. For the Pt/C_{HPM} and commercial Pt/C catalyst, they were obtained below 0.6 V with an electrode angular speed at 1600 rpm. However, it was not achieved for the Pt/C_{DEL} catalyst, as shown in Fig. 10(b). The limited performance of the Pt/C_{DEL} catalyst was due to the limited active surface area and reactant access to the catalyst due to the additional limitation of the pores in the dense material and the aggregation of the catalyst support during measurement degrades

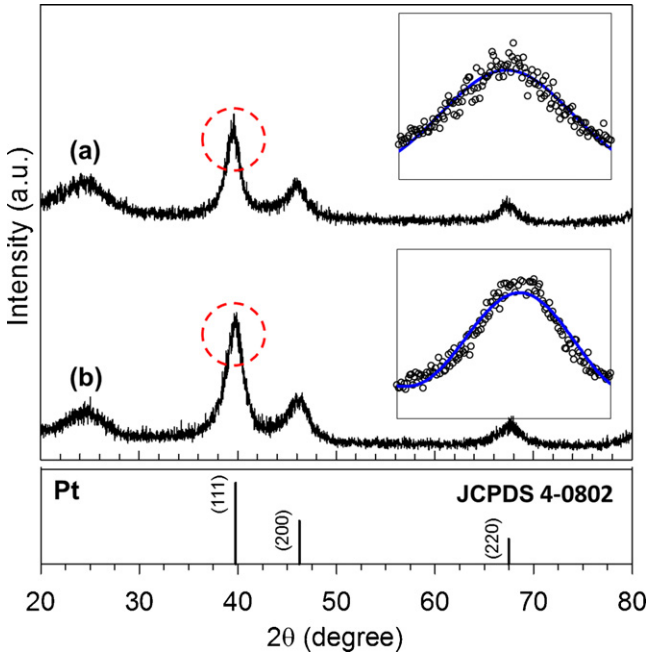

Fig. 7. XRD patterns for Pt/C catalyst after reheated at 120 °C for 120 min under vacuum: (a) DEL and (b) HPM.

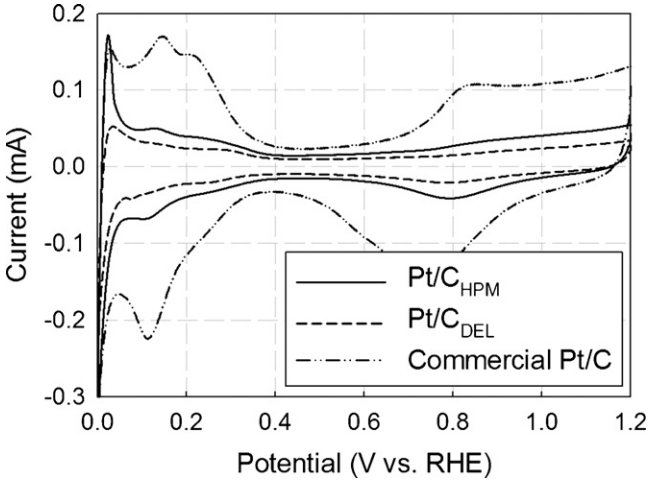

Fig. 8. Cyclic voltammogram of various catalyst samples in O_2-free 0.1 M $HClO_4$ (cycling between 0 and 1.2 V at 50 mV s^{-1} sweep rate).

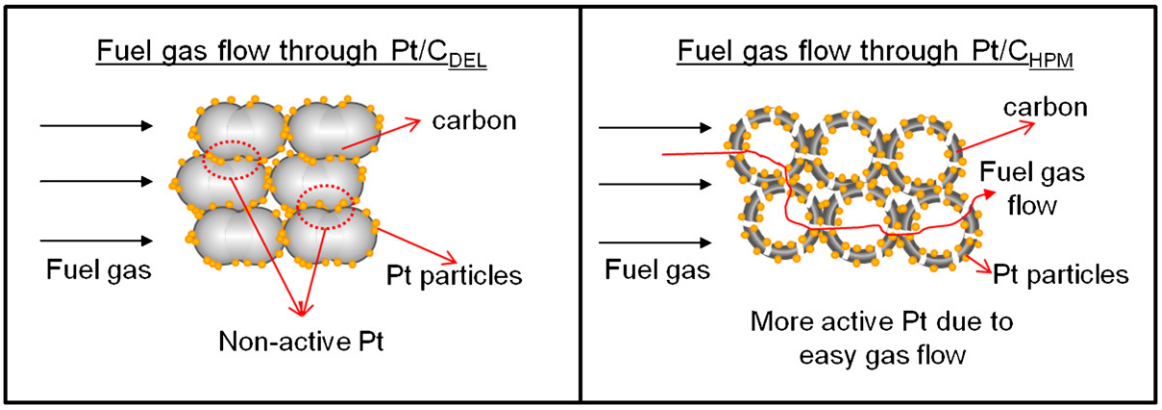

Fig. 9. Schematic diagram of fuel gas flow through Pt/C_{DEL} and Pt/C_{HPM} and its contact with the Pt catalyst.

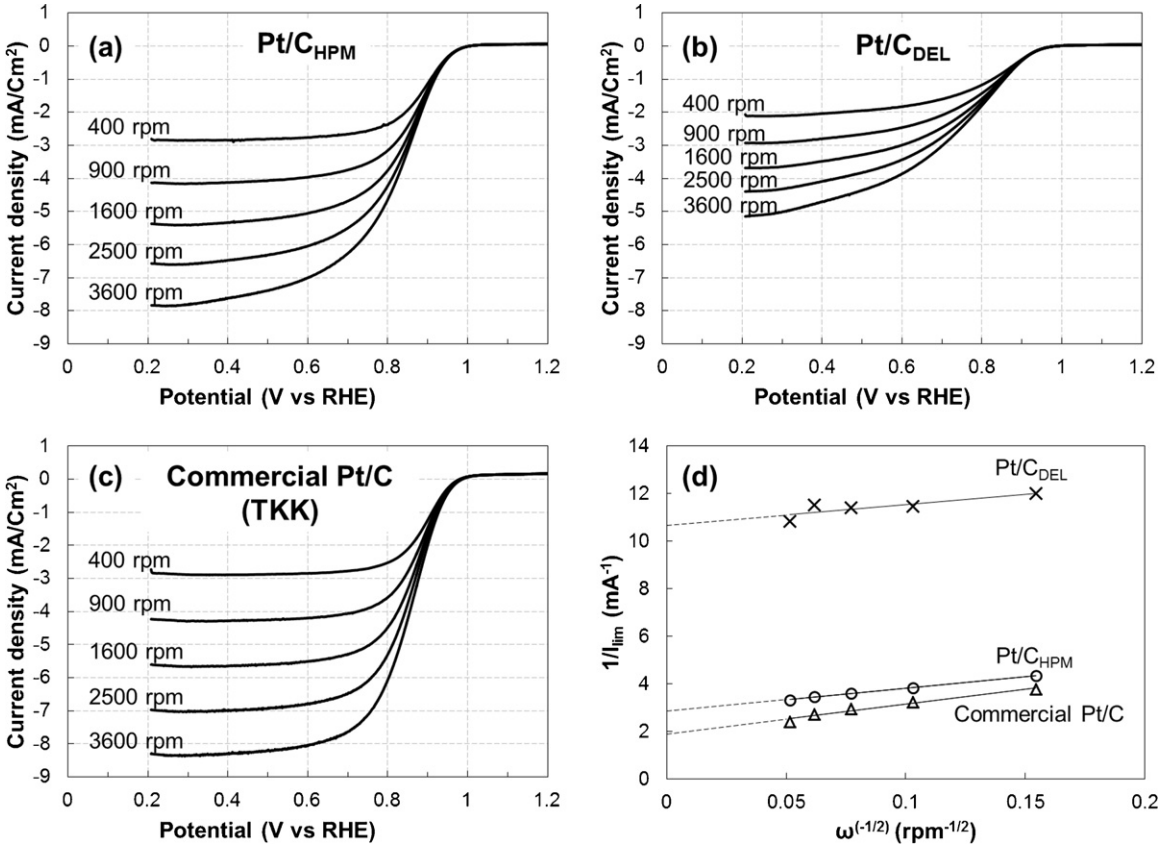

Fig. 10. (a–c) ORR polarization curves at different rotation rates for Pt/C_{HPM}, Pt/C_{DEL}, and commercial Pt/C, respectively, in O_2 saturated 0.1 M $HClO_4$ at sweep rate 10 mV s^{-1} and (d) Koutecký–Levich plot of Pt/C_{HPM}, Pt/C_{DEL}, and commercial Pt/C at 1600 rpm.

the performance, which is responsible for the loss of the platinum nanoparticles from the electrical contact. As for Pt/C_{HPM} catalyst, the channel morphology still provides an access for Pt catalyst even though aggregation of the catalyst support occurs as illustrated in Fig. 9. Target potential for the calculation of the mass activity and specific activity was quantified at $E = 0.9$ V. At $E < 0.9$, interferences from mass-transport losses (diffusion limited current density) take place partially due to the effect of the presence of nafion, meanwhile at $E > 0.9$, the current density measurement was very close to the open-circuit voltage condition [30,40]. The mass activity and specific activity were evaluated from Koutecký–Levich plot (Fig. 10d), using the limiting current method. The limiting current for each electrode is tabulated in Table 1. Pt mass activities were calculated by normalizing the Pt loading of the disk electrode and the specific activities were estimated by calculating the mass-specific activities and normalizing them to the Pt electrochemical surface area. The mass activities of the Pt/C_{DEL}, Pt/C_{HPM}, and commercial Pt/C catalysts were 86.80, 239.57, and 155.01 mA mg^{-1} Pt,

Table 1
Limiting current (mA) of Pt/C_{HPM}, Pt/C_{DEL}, and commercial Pt/C measured at 0.9 V at different rotation speeds.

Sample	Rotation speed of RDE (rpm)				
	400	900	1600	2500	3600
Pt/C_{HPM}	−0.2305	−0.2612	−0.2768	−0.288	−0.3006
Pt/C_{DEL}	−0.0832	−0.0872	−0.0876	−0.0869	−0.0923
Commercial Pt/C	−0.2651	−0.3095	−0.3391	−0.3681	−0.4146

Table 2
Catalyst characterization results.

Sample	Pt size (nm)	Pt loading (wt.%)	Pt amount on RDE ($\mu g\,Pt\,cm^{-2}$)	ECSA ($m^2\,g^{-1}$ Pt)	Mass activity ($mA\,mg^{-1}$ Pt)	Specific activity ($\mu A\,cm^{-2}$ Pt)
Pt/C_{DEL}	~3.94	7.3	7.4	40.98	86.80	211.80
Pt/C_{HPM}	~3.88	9.9	5.5	54.18	239.57	442.19
Commercial Pt/C	~2–3	46.1	17.3	80.47	155.01	192.61

respectively, whereas their specific activities were 211.80, 442.19, and 192.61 $\mu A\,cm^{-2}$ Pt, respectively.

The prepared Pt/C_{HPM} catalyst showed great promise for PEMFC applications with its improved properties such as higher mass activity and specific activity than that of its commercial counterparts as summarized in Table 2. Those improvements were achieved due to the hollow-porous structures. The porous shell was critical, because the permeable layer allowed the species to be transported between the macroporous core and the exterior of the particles, thus enlarging the three phase boundary among catalyst, gas phase, and electrolyte. This morphology allowed effective gas/water diffusion and proton/electron transport to and from the catalyst sites. The appropriate size of Pt also played a role in this achievement. Reportedly, particle size has a significant effect on ORR activity, and the optimum particle size is around 4 nm [41], which is in agreement with the results of the present study.

4. Conclusion

The present study demonstrated a facile strategy to design Pt/C catalysts for high-performance PEMFCs applications. High-performance PEMFCs could be achieved by engineering the structure of the catalyst support materials to obtain a hollow-porous-microsphere structure. The Pt/C_{HPM} catalyst showed improved electrochemical performance compared to the commercial Pt/C catalyst. The combination of low Pt amount, simplicity in its preparation, and excellent electrochemical properties shows great promise for the present study as a method of preparation for Pt/C catalyst for high-performance fuel cell applications.

Acknowledgement

The authors would like to thank to Dr. Eishi Tanabe from the Hiroshima Prefectural Institute of Industrial Science and Technology for helping with the TEM analysis, Prof. Tsuneji Sano for the help on the BET measurement, and The Ministry of Education, Culture, Sports, Science and Technology (MEXT) of Japan for providing a doctoral scholarship for R.B.

Appendix A. Supplementary data

Supplementary data associated with this article can be found, in the online version, at doi:10.1016/j.jpowsour.2011.11.064.

References

[1] B. Fang, N.K. Chaudhari, M.-S. Kim, J.H. Kim, J.-S. Yu, J. Am. Chem. Soc. 131 (2009) 15330–15338.
[2] Z. Liua, L.M. Gana, L. Honga, W. Chen, J.Y. Lee, J. Power Sources 139 (2005) 73–78.
[3] A.V. Virkar, Y. Zhou, J. Electrochem. Soc. 154 (2007) 540–547.
[4] Y.-H. Shih, G.V. Sagar, S.D. Lin, J. Phys. Chem. C 112 (2008) 123–130.
[5] T. Ghosh, B.M. Leonard, Q. Zhou, F.J. DiSalvo, Chem. Mater. 22 (2010) 2190–2202.
[6] Y. Bing, H. Liu, L. Zhang, D. Ghosh, J. Zhang, Chem. Soc. Rev. 39 (2010) 2184–2202.
[7] B. Lim, M. jiang, P.H.C. Camargo, E.C. Cho, J. Tao, X. Lu, Y. Zhu, Y. Xia, Science 324 (2009) 1302–1305.
[8] A.C. Fernandes, V.A. Paganin, E.A. Ticianelli, J. Electroanal. Chem. 648 (2010) 156–162.
[9] S.C. Zignania, E. Antolini, E.R. Gonzalez, J. Power Sources 191 (2009) 344–350.
[10] J.B. Joo, P. Kim, W. Kim, J. Appl. Electrochem. 39 (2009) 135–140.
[11] S. Pylypenko, T.S. Olson, N.J. Carroll, D.N. Petsev, P. Atanassov, J. Phys. Chem. C 114 (2010) 4200–4207.
[12] Y.S. Yun, H. Bak, H.-J. Jin, Synthetic Met. 160 (2010) 561–565.
[13] B. Fang, J.H. Kim, M. Kim, M. Kim, J.-S. Yu, Phys. Chem. Chem. Phys. 11 (2009) 1380–1387.
[14] J.H. Kim, J.-S. Yu, Phys. Chem. Chem. Phys. 12 (2010) 15301–15308.
[15] Z. Qu, W. Huang, S. Zhou, H. Zheng, X. Liu, M. Cheng, X. Bao, J. Catal. 234 (2005) 33–36.
[16] A. Stein, Z. Wang, M.A. Fierke, Adv. Mater. 21 (2009) 265–293.
[17] T. Soboleva, X. Zhao, K. Malek, Z. Xie, T. Navessin, S. Holdcroft, Appl. Mater. Interfaces 2 (2010) 375–384.
[18] J.H. Bang, K. Han, S.E. Skrabalak, H. Kim, K.S. Suslick, J. Phys. Chem. C 111 (2007) 10959–10964.
[19] B. Fiçicilar, A. Bayrakçeken, İ. Eroğlu, Int. J. Hydrogen Energ. 35 (2010) 9924–9933.
[20] M. Watanabe, K. Makita, H. Usami, S. Motoo, J. Electroanal. Chem. 197 (1986) 195–208.
[21] M. Uchida, Y. Aoyama, N. Eda, A. Ohta, J. Electrochem. Soc. 142 (1995) 4143–4149.
[22] M. Uchida, Y. Fukuoka, Y. Sugawara, N. Eda, A. Ohta, J. Electrochem. Soc. 143 (1996) 2245–2252.
[23] N. Job, S. Lambert, M. Chatenet, C.J. Gommes, F. Maillard, S. Berthon-Fabry, J.R. Regalbuto, J.-P. Pirard, Catal. Today 150 (2010) 119–127.
[24] A.M. Chaparro, M.A. Folgado, P. Ferreira-Aparicio, A.J. Martín, I. Alonso-Álvarez, L. Daza, J. Electrochem. Soc. 157 (2010) 993–999.
[25] Q. Wang, M. Eikerling, D. Song, Z. Liu, J. Electroanal. Chem. 573 (2004) 61–69.
[26] Z.-B. Wang, C.-R. Zhao, P.-F. Shi, Y.-S. Yang, Z.-B. Yu, W.-K. Wang, G.-P. Yin, J. Phys. Chem. C 114 (2010) 672–677.
[27] J.H. Kim, B. Fang, M. Kim, J.-S. Yu, Catal. Today 146 (2009) 25–30.
[28] M.L. Anderson, R.M. Stroud, D.R. Rolison, Nano Lett. 2 (2002) 235–240.
[29] R. Balgis, F. Iskandar, T. Ogi, A. Purwanto, K. Okuyama, Mater. Res. Bull. 46 (2011) 708–715.
[30] Y. Garsani, O.A. Baturina, K.E. Swider-Lyons, S.S. Kocha, Anal. Chem. 82 (2010) 6321–6328.
[31] O.D. Velev, A.M. Lenhoff, E.W. Kaler, Science 287 (2000) 2240–2243.
[32] F. Iskandar, L. Gradon, K. Okuyama, J. Colloid Interf. Sci. 265 (2003) 296–303.
[33] N. Passe-Coutrin, S. Altenor, D. Cossement, C. Jean-Marius, S. Gaspard, Micropor. Mesopor. Mater. 111 (2008) 517–522.
[34] S. Singh, J. Datta, J. Mater. Sci. 45 (2010) 3030–3040.
[35] W. Chena, Y. Tang, J. Bao, Y. Gao, C. Liu, W. Xing, T. Lu, J. Power Sources 167 (2007) 315–318.
[36] T.J. Schmidt, H.A. Gasteiger, G.D. Stab, P.M. Urban, D.M. Kolb, R.J. Behm, J. Electrochem. Soc. 145 (1998) 2354–2358.
[37] S.St. John, I. Dutta, A.P. Angelopoulos, Langmuir 27 (2011) 5781–5791.
[38] E. Antolini, J. Mater. Sci. 38 (2003) 2995–3005.
[39] C. Grolleau, C. Coutanceau, F. Pierre, J.-M. Léger, Electrochim. Acta 53 (2008) 7157–7165.
[40] W.J. Khudhayer, N.N. Kariuki, X. Wang, D.J. Myers, A.U. Shaikh, T. Karabacak, J. Electrochem. Soc. 158 (2011) 1029–1041.
[41] C.W.B. Bezerra, L. Zhang, H. Liu, K. Lee, A.L.B. Marques, E.P. Marques, H. Wang, J. Zhang, J. Power Sources 173 (2007) 891–908.